ACS APPLIED MATERIALS & INTERFACES

www.acsami.org

Research Article

Two Competing Reactions of Sulfurized Polyacrylonitrile Produce High-Performance Lithium−Sulfur Batteries

Huilan Li, Wenying Xue, Lina Wang,* and Tianxi Liu

Cite This: *ACS Appl. Mater. Interfaces* 2021, 13, 25002−25009

Read Online

ACCESS | Metrics & More | Article Recommendations | Supporting Information

ABSTRACT: Sulfurized polyacrylonitrile (SPAN) is an attractive cathode candidate for the advanced lithium−sulfur (Li−S) batteries owing to its outstanding cyclic stability. Nevertheless, SPAN suffers from inadequate initial Coulombic efficiency (CE) induced by the sluggish reaction kinetics, which is primarily ascribed to the low Li-ion diffusivity and high electronic resistivity of the Li_2S product. In this work, an optimal trace amount of soluble lithium polysulfide of Li_2S_8 is introduced as a redox mediator for a freestanding fibrous SPAN cathode to enhance the reversible oxidation efficiency of Li_2S. During the delithiation process, the chemical interactions between Li_2S and Li_2S_8 additive facilitate the electrochemical oxidation of Li_2S, resulting in the transformation of not only C−S/S−S bonds in SPAN but also elemental sulfur. Benefiting from the synergistic effect of the two competing reactions, a high initial CE of 82.9% could be achieved at a current density of 200 mA g^{-1}. Moreover, a superior capacity retention along with a high capacity of 1170 mAh g^{-1} up to the 400th cycle is available at 1000 mA g^{-1}. The study offers a feasible approach for Li−S batteries toward the practical applications of SPAN.

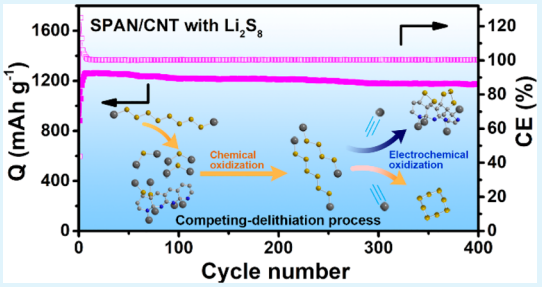

KEYWORDS: *sulfurized polyacrylonitrile, nanofibers, lithium polysulfides, competing reactions, fast reaction kinetics*

1. INTRODUCTION

A rechargeable lithium−sulfur (Li−S) battery is competitive among the developing power sources owing to a high theoretical energy density (2600 Wh kg^{-1}) and the environmental benignity of elemental sulfur (S_8).[1−4] Nevertheless, the practical use of a S_8 cathode was blocked by the unsatisfactory capacity retention and self-discharge. Besides the insulating nature of both S_8 and the final Li_2S discharge product[5−7] and a volume expansion of 70−80% from the conversion of S_8 to Li_2S,[8,9] the nonelectrochemical shuttle of soluble polysulfide intermediates (Li_2S_n, $2 < n \leq 8$) is mainly responsible for the poor battery performance.[10−12] Diverse approaches, including encapsulating sulfur into the conductive porous frameworks,[13−17] anchoring polysulfides on polar sites,[8,18−25] etc., have been conducted. Indeed, it is thermodynamically unavoidable with respect to the diffusion of the continuously generated soluble polysulfides with S_8 cathodes in liquid electrolytes.

Sulfurized polyacrylonitrile (SPAN) as an alternative cathode material to S_8 has been highly attractive to realize practical Li−S batteries since that first reported by Wang et al.[26] Through the heat-treatment, polyacrylonitrile (PAN) polymer chains are dehydrogenated and cyclized by losing hydrogen sulfide, and the resulting carbon double bonds are instantly sulfurized by small sulfur fragments.[27−31] The SPAN has shown high chemical compatibility with carbonate-based electrolytes, exhibiting superior cyclic stability and extremely low self-discharge. Therefore, it is generally believed that a solid-phase electrochemical conversion of SPAN ↔ Li_2S takes place in carbonates. Whereas, SPAN has demonstrated poor compatibility with ether electrolytes due to the spontaneous transformation of Li_2S_n.[27,31−34] However, the Li anodes have been proven to have a higher cyclic efficiency and a lower voltage hysteresis in ether-based electrolytes. The different compatibilities of a SPAN cathode and a Li anode with electrolytes would limit the practical use of the system.

Recently, we demonstrated a freestanding fibrous SPAN cathode that is compatible with not only carbonate but also ether electrolytes.[35] The rational molecular structure indicates that the short $-S_2-$ and $-S_3-$ chains are bonded to adjacent carbon atoms of the backbone. The solid-phase conversion between SPAN nanofibers and Li_2S product without generation of soluble Li_2S_n was also realized in ether electrolytes. However, the SPAN suffers from unsatisfactory Coulombic efficiency (CE, defined as $Q_{charge}/Q_{discharge}$) on the first cycle, and there is still space for further improvement of the rate capability.[35] In a review of previous reports that have

Received: April 1, 2021
Accepted: May 12, 2021
Published: May 20, 2021

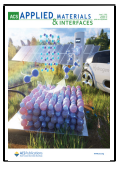

https://doi.org/10.1021/acsami.1c06004
ACS Appl. Mater. Interfaces 2021, 13, 25002−25009

provided CE information, the SPAN materials that cycled in carbonate electrolytes have also shown problems.[34,36−44] An initial CE value <75% was generally presented irrespective of the morphology of the SPAN.[34,36−44] For instance, the powdery SPAN material reported by Wang et al. exhibited an initial CE of 62% at 50 mA g^{-1}.[34] That reported by Jerez et al. showed an initial CE of 64.7% at a current rate of 0.1 C (1 C = 1675 mA g^{-1}).[38] Some fibrous SPAN materials are no exception.[42−44] Ye et al. reported SPAN nanofibers with an initial CE of 56.9% at 200 mA g^{-1}.[42] Kim et al. prepared a fibrous SPAN network with an initial CE of 54.9% at 0.01 C.[44] The electrochemically irreversible processes of the reduction via C−Li/N−Li on the graphitized backbone[35,45−48] have been recognized as one reason. The other main reason is the sluggish reaction kinetics induced by the high delithiation energy barrier of Li_2S. The residual Li_2S after the initial reverse charge was clearly detected by morphological and spectroscopic techniques in our previous work.[35] To accelerate the interfacial charge transfer between the pyrolytic backbone and Li_2S is crucial for a higher charge/discharge efficiency. To address this issue, one critical factor is to enhance the electronic conductivity of the polymer backbone. For example, the initial CE is only 21.6% at 200 mA g^{-1} for the neat SPAN nanofibers that were synthesized at 350 °C (Figure S1). By introducing carbon nanotubes (CNTs) into the nanofibers as conductive fillers, the initial CE is increased to 30.1%.[35] By further increasing the sulfuration temperature from 350 to 500 °C for a higher graphitization of the backbone, an initial CE of 77% can be reached. The other key point is to overcome the high Li-ion diffusive resistivity on the surface of Li_2S. The mechanism is similar to the sluggish delithiation kinetics of Li_2O_2 as the insulating product of lithium−oxygen (Li−O_2) batteries.[49−51] Involving redox mediators (RMs) is an effective strategy to overcome the difficulty.[52−54] Depending on the electrochemical redox of RMs in solution, Li_2O_2 in turn can be chemically oxidized on the surface. The trials of RMs in Li−S cells have been limited to that with a S_8 or Li_2S cathode.[55,56] For example, 3,4,9,10-perylenetetracarboxylic diimide was utilized as an RM to enhance the conversion speed from polysulfides to S_8.[56] Yang et al. first discovered that Li_2S can be electrochemically activated directly as a cathode by overcoming a potential barrier at an early stage of the initial charge.[57] Such an initial potential barrier disappeared in a polysulfide-containing electrolyte for a reduced extra free energy of phase nucleation. The reaction mechanism of the SPAN cathode with the discharge product of Li_2S is a different case. How to accelerate the solid-phase conversion kinetics between SPAN and Li_2S effectively to promote energy efficiency is still a critical challenge of the system.

Herein, a controlled trace amount of Li_2S_8 is introduced in ether-based electrolytes as a chemical mediator in the lithium battery with a freestanding fibrous SPAN cathode. The solid Li_2S nanoflakes produced during discharge can be activated in two ways on recharge. Li_2S_8 would react with Li_2S chemically to generate lithium polysulfides (Li_2S_n, $4 \leq n < 8$), which can be further electrochemically oxidized to SPAN or S_8 simultaneously. The combined morphological, spectroscopic, and electrochemical characterizations reveal that the two competing reactions promote the reversible delithiation efficiency of Li_2S. Benefiting from the unique reaction mechanism, the SPAN delivers a high initial CE of 82.9% at 200 mA g^{-1}, improved capability at high current rates, and a decent long-term cycle life.

2. EXPERIMENTAL SECTION

2.1. Preparation of a Freestanding Fibrous SPAN/CNT Electrode. The precursor PAN/CNT films were prepared by electrospinning.[35] Appropriate amounts of PAN (M_w = 150 000, Sigma-Aldrich) and CNTs (multiwalled, 98% purity, diameter (d) = 10−20 nm) were added in *N*,*N*-dimethylformamide (DMF, 99.5%, Shanghai Lingfeng Chemical) at room temperature for 12 h of continuous stirring. The resultant solution was then loaded into a syringe with a needle and electrospun onto the aluminum foil collector at 1.6 mL h^{-1}. A high voltage of 18 kV was applied to the metallic needle with a distance of 24 cm from the needle to the collector. Finally, the PAN/CNT nanofiber films below a layer of sublimed sulfur (chemical purity, Sinopharm Chemical) were heated at 500 °C for 3 h to get SPAN/CNT. The sulfur was in excess for a thorough sulfuration of PAN. A pPAN/CNT sulfur-free film was prepared by pyrolysis of PAN/CNT at 500 °C as a controlled sample.

2.2. Preparation of Electrolytes. The base electrolyte is 1,3-dioxolane/1,2-dimethoxyethane (DOL/DME, 1/1, v/v) containing 0.2 M $LiNO_3$ (Shanghai Songjing Energy Co., Ltd.) and 1 M lithium bis(trifluoromethanesulfone)imide (LiTFSI). The polysulfide-containing electrolyte was prepared by reacting commercial Li_2S (99.9%, Alfa Aesar) and sublimed sulfur (1:7 of Li_2S to S by mole ratio) in the base electrolyte to form Li_2S_8. The base electrolyte in the presence of 0.07 M Li_2S_8 was prepared for electrochemical characterizations.

2.3. Electrochemical Measurements. The freestanding SPAN/CNT nanofiber films were cut into discs of 12 mm in diameter and used as a cathode directly. As a control, a conventional sulfur cathode that was denoted as pPAN-S_8/CNT was prepared from a *N*-methyl-2-pyrrolidone (NMP, ≥99.0%) slurry involving 40 wt % elemental sulfur, 30 wt % pPAN/CNT, 20 wt % Ketjenblack carbon (KB, ECP-600JD), and 10 wt % polyvinylidene fluoride (PVdF, HSV900). The electrode with an Al foil (18 μm thick) current collector was obtained after being dried overnight in a vacuum oven at 50 °C. Normally, the sulfur loading (calculated based on the mass of S) in SPAN/CNT and pPAN-S_8/CNT cathodes was controlled to be ca. 2 mg cm^{-2}. The electrolyte in each cell was controlled the same, at ∼40 μL. Therefore, the electrolyte volume-to-active sulfur mass ratio, which is generally presented as E/S, is 17.7 μL mg^{-1}. Coin cells were assembled in a glovebox (Mikrouna) under argon atmosphere with H_2O and O_2 of <1 ppm. The separator is a polypropylene/polyethylene (PP/PE) microporous membrane (Celgard 2325) with an 18 mm diameter, and the anode is Li metal with a 14 mm diameter. The galvanostatic cylic measurements were performed on a LAND battery test system (Wuhan, China) within a cutoff voltage of 1.0−3.0 V at room temperature, 25 °C. The cyclic voltammograms (CVs) were tested on an Arbin electrochemical workstation (U.S.A.) at a sweep rate of 0.05 mV s^{-1}. The electrochemical impedance spectroscopy (EIS) was tested on a Chenhua CHI660E workstation (Shanghai) within a frequency of 0.1 Hz−100 kHz.

2.4. Material Characterizations. Field-emission scanning electron microscopy (FE-SEM, S-4800, Hitachi), transmission electron microscopy (TEM, JEM-2100F, JEOL), and energy-dispersive X-ray spectroscopy (EDS) were combined for the morphological study. The crystal structure was detected by an X-ray diffractometer (XRD, D/max-2550VB+/PC, Rigalcu) equipped with Cu Kα radiation. Fourier transform infrared (FTIR) spectra were recorded on a Bruker VECTOR22 FTIR spectrometer. Raman spectra were obtained by an inVia Reflex Raman Spectrometer (inVia-Reflex, Renishaw). The elemental content was evaluated by an elemental analyzer (Vario EL III, Elementar, Germany). The thermal gravimetric analysis (TGA, NETZSCH TG 209 F1 Libra) was performed from ambient temperature to 1000 °C in N_2 atmosphere. X-ray photoelectron spectroscopy (XPS, Escalab 250Xi) was recorded with a monochromatic Al Kα X-ray source.

3. RESULTS AND DISCUSSION

The preparation of freestanding fibrous SPAN/CNT cathodes involves a facile two-step process.[35] First, the DMF solution

https://doi.org/10.1021/acsami.1c06004
ACS Appl. Mater. Interfaces 2021, 13, 25002−25009

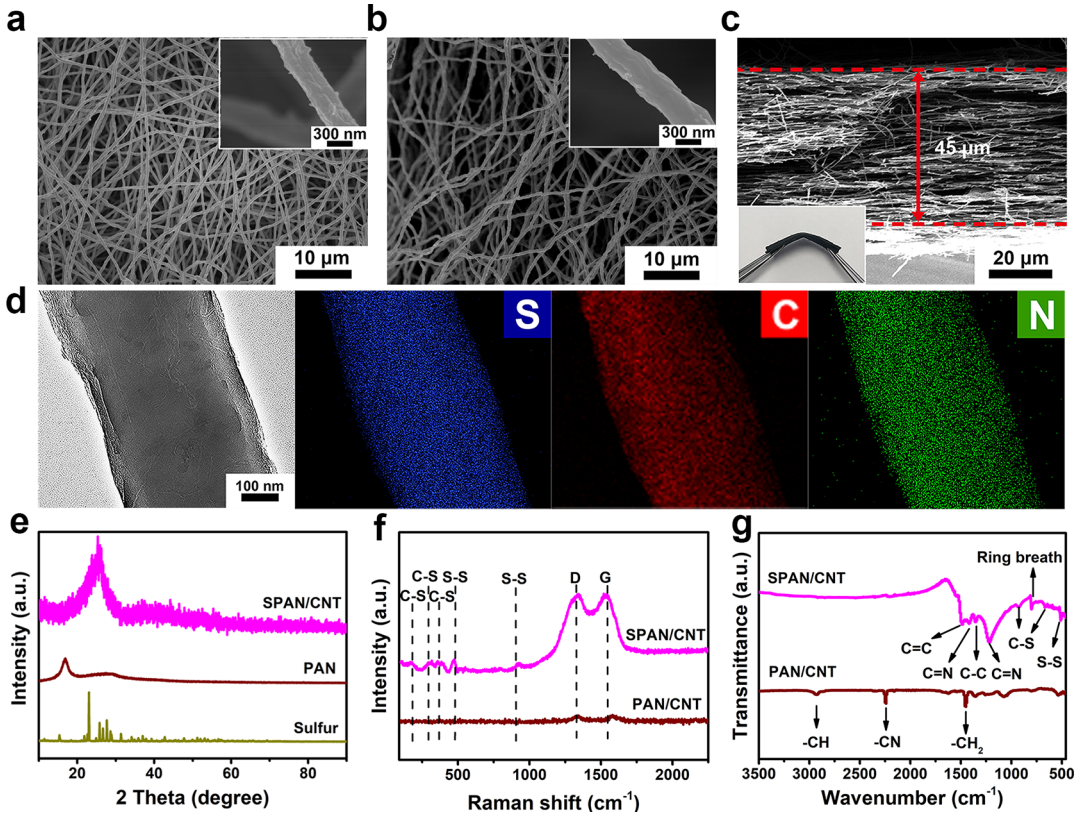

Figure 1. Top-view SEM images of (a) PAN/CNT precursor film and (b) SPAN/CNT film. The inset is the image of single nanofiber. (c) Cross-sectional image of the SPAN/CNT film. The inset is a digital picture of the flexible and freestanding electrode. (d) TEM image of single SPAN/CNT nanofiber and the corresponding elemental mappings. (e) XRD patterns of SPAN/CNT, PAN, and elemental sulfur. (f) Raman and (g) FTIR spectra of SPAN/CNT and PAN/CNT.

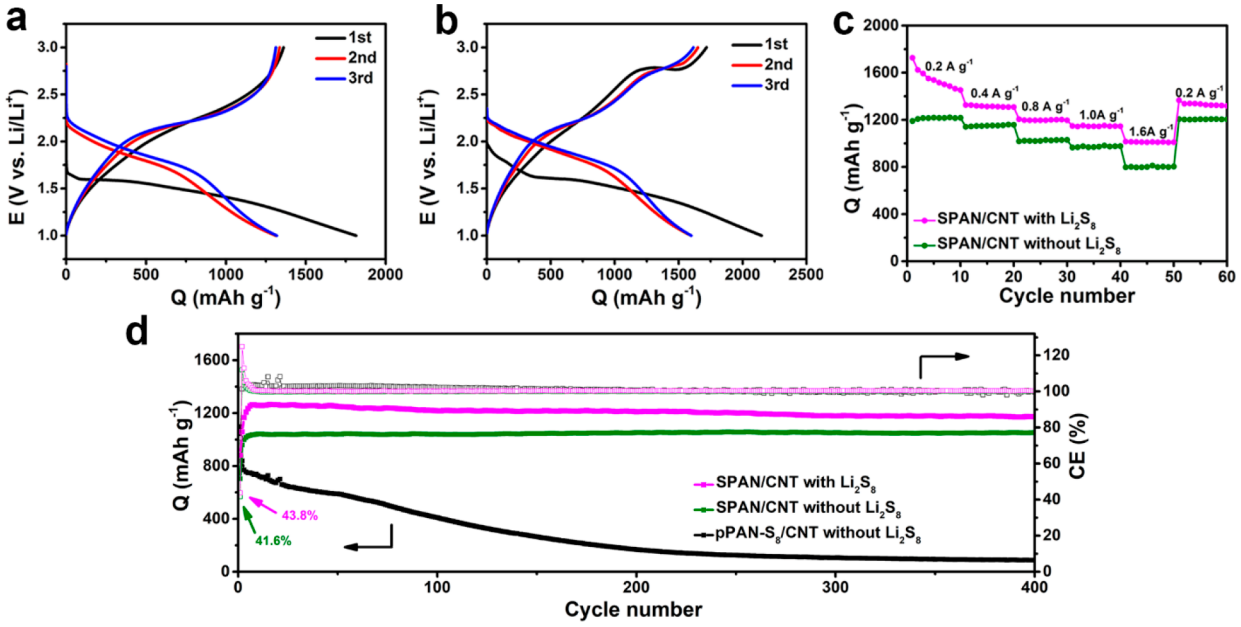

Figure 2. Discharge−charge profiles of SPAN/CNT (a) in the base ether electrolyte and (b) in the Li_2S_8-containing ether electrolyte at 400 mA g^{-1}. (c) Rate capability of SPAN/CNT in the ether-based electrolyte with or without Li_2S_8 additive. (d) Cyclic performances of SPAN/CNT and pPAN-S_8/CNT in the ether-based electrolyte with or without Li_2S_8 additive at 1000 mA g^{-1}.

containing PAN and CNTs was electrospun into a PAN/CNT precursor film. Then, the film was heated with S_8 under a nitrogen atmosphere for sulfuration at 500 °C. FE-SEM images show that the interconnected network of PAN/CNT nanofibers (Figure 1a) is maintained after sulfuration (Figure 1b). In contrast to PAN/CNT nanofibers of ca. 400 nm in diameter (inset in Figure 1a), the SPAN/CNT nanofibers are found to inflate in diameter (ca. 500 nm, inset in Figure 1b), resulting

https://doi.org/10.1021/acsami.1c06004
ACS Appl. Mater. Interfaces 2021, 13, 25002−25009

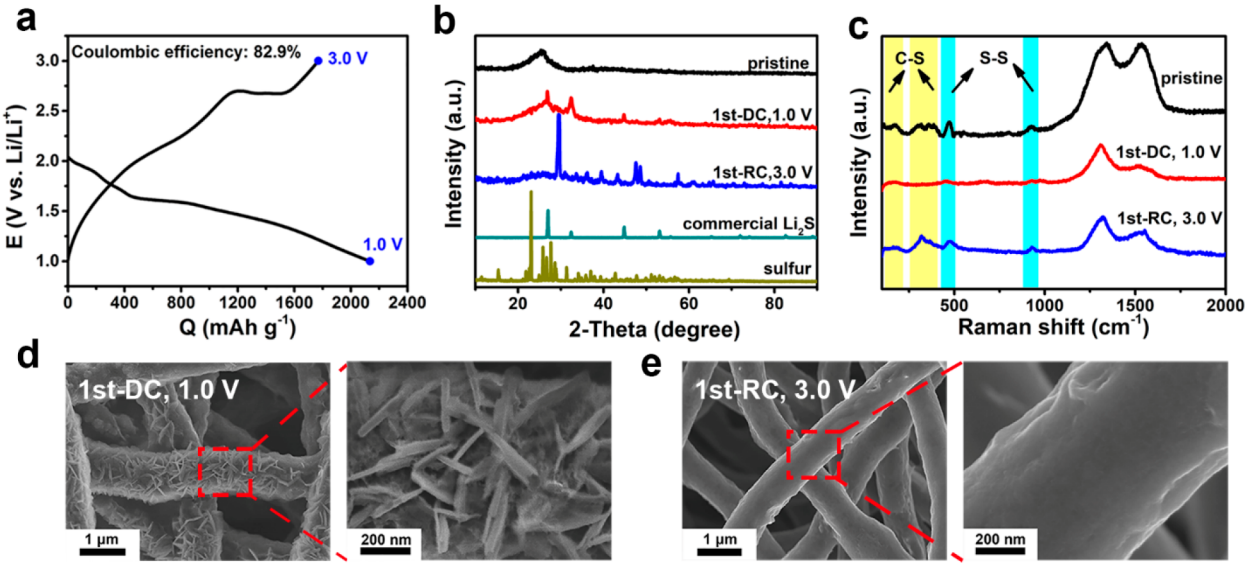

Figure 3. (a) Initial discharge−charge profile of SPAN/CNT in the Li_2S_8-containing ether electrolyte at 200 mA g^{-1}. The corresponding ex situ (b) XRD patterns and (c) Raman spectra of of SPAN/CNT electrodes at pristine state, first discharged to 1.0 V (1st-DC), and first recharged to 3.0 V (1st-RC). SEM images of the (d) 1st-DC and (e) 1st-RC SPAN/CNT electrodes.

from the saturated infiltration of the sulfur species. The 40 ± 5 μm thick film could be bent easily without any damage (Figure 1c), revealing its robust and flexible structure. The sulfur content of SPAN/CNT is 37.6 wt % (Table S1). The homogeneous distribution of S, C, and N elements throughout the nanofibers is confirmed by EDS elemental mapping images (Figure 1d).

XRD patterns reveal the crystallinity of SPAN/CNT (Figure 1e). The characteristic diffraction of elemental sulfur between 10° and 70° and that of PAN at 17° are not observed in the pattern of SPAN/CNT, indicating that sulfur exists in an amorphous state. A new broad peak at 26.5° in accordance with the graphitic (002) plane verifies the graphitization of the polymer backbone. In Raman spectra, the characteristic peaks at 1325 and 1540 cm^{-1} are ascribed to the disordered D band and the graphitic G band in carbonaceous materials, respectively (Figure 1f). Compared to PAN/CNT, the SPAN/CNT shows characteristic C−S/S−S signals. The peaks at 176, 298, and 370 cm^{-1} are associated with C−S groups, and those at 466 and 925 cm^{-1} are signals of S−S stretch.[35,58,59] The FTIR spectrum of PAN/CNT exhibits bands corresponding to −CH, −CN, and $-CH_2$ groups at 2936, 2243, and 1452 cm^{-1}, respectively (Figure 1g). The C═C, C═N, C−S, and S−S bonds are detected instead in the FTIR spectrum of SPAN/CNT, suggesting the successful sulfuration of PAN/CNT.[32,49,60] The signals at 1495 and 1235 cm^{-1} are indexed to the symmetric stretch of C═C and C═N bonds, respectively,[29,35] and that at 802 cm^{-1} responds to the ring-breathing vibration of hexahydric rings.[33] The absence of elemental sulfur in SPAN/CNT is further confirmed by TGA (Figure S2). In contrast to elemental sulfur, which undergoes a 100% weight loss in 180−300 °C, the SPAN/CNT starts to lose weight beyond 600 °C, reflecting that S atoms are covalently bonded to the backbone. These results confirm the successful synthesis of the SPAN/CNT composite.

To reduce the energy barrier of the reverse conversion from Li_2S product to SPAN, a trace amount of Li_2S_8 additive (0.07 M) was employed in the ether of a DOL/DME-based electrolyte. The role of Li_2S_8 was first assessed in terms of the galvanostatic charge−discharge test. In the Li_2S_8-free electrolyte, the SPAN/CNT features a high discharge capacity of 1814 mAh g^{-1}, a long output plateau at 1.6 V (vs Li/Li^+), and a CE of 74.9% on the first cycle when operating at 400 mA g^{-1} (Figure 2a). Upon the following cycles, the reduced voltage hysteresis and almost 100% CE suggest the improved reaction kinetics. However, the lost reversible capacity upon the first cycle has never been recovered. As for the SPAN/CNT with the Li_2S_8-containing electrolyte, a relatively higher initial CE of 79.9% is achieved (Figure 2b). Significantly, one pair of additional plateaus appears at 2.3 and 2.8 V in the voltage profiles, which is consistent with the CV curves (Figure S3). Furthermore, the SPAN/CNT with Li_2S_8 in the electrolytes delivers a higher reversible capacity of 1452−1009 mAh g^{-1} at different current densities of 200−1600 mA g^{-1}, respectively (Figure 2c). Compared to the fresh cell with base electrolyte, the one with the Li_2S_8-added electrolyte exhibits a lower interfacial charge-transfer resistance, suggesting accelerated reaction kinetics (Figure S4). The enhanced initial CEs at various current rates provide further convincing evidence of the enhanced interfacial charge transfer between Li_2S and the polymer backbone (Figure S5). The long-term operation at 1000 mA g^{-1} suggests that a trace of Li_2S_8 additive would not destroy the decent cyclic performance (Figure 2d). A specific capacity of 1170 mAh g^{-1} is achieved after stable cycling for 400 cycles. Such a cell performance of the SPAN/CNT with the Li_2S_8-containing electrolyte is among the impressive results shown in a review of previous SPAN-based electrodes (Table S2). To increase the sulfur loading to ca. 4.0 mg cm^{-2} with a layer-by-layer configuration,[35] a stable cycling and a capacity of 1115 mAh g^{-1} at the 100th cycle is still available (Figure S6). The same use of a combination of the Li_2S_8-containing electrolyte with a freestanding pPAN/CNT cathode by pyrolyzation of PAN/CNT leads to a capacity no higher than 50 mAh g^{-1} (Figure S7). Therefore, the capacity that the Li_2S_8 additive contributed was not calculated in the SPAN/CNT system.

From the different electrochemical characteristics, it is known that there is an intrinsically different reaction

https://doi.org/10.1021/acsami.1c06004
ACS Appl. Mater. Interfaces 2021, 13, 25002−25009

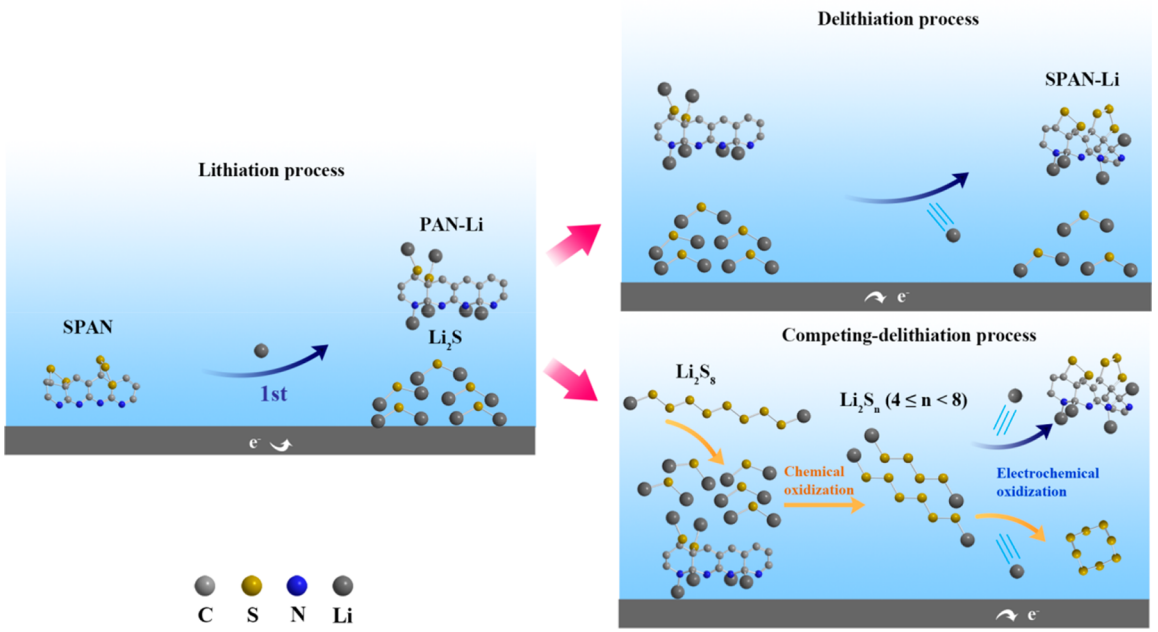

Figure 4. Schematic of the lithiation process of SPAN/CNT nanofibers and the two different delithiation processes of Li_2S in base or Li_2S_8-containing ether electrolyte.

mechanism of SPAN/CNT in the base and the Li_2S_8-added electrolytes. The improved initial CE and rate capability indicate that the Li_2S_8 additive boosts the reaction kinetics. The discharge−charge profiles suggest that the SPAN in the Li_2S_8-containing electrolyte undergoes a different reaction mechanism from the solid-state conversion reaction in the base electrolyte. The reaction is also distinguished from the solid−liquid−solid conversion of S_8. The pPAN-S_8/CNT prepared from the slurry-casting method of the mixed pPAN/CNT and S_8 exhibits typical stepwise discharge plateaus, which corresponds to the sequential reduction of $S_8 \rightarrow Li_2S_n \rightarrow Li_2S$ (Figure S8a). Because of the uncontrolled internal shuttle of Li_2S_n, the pPAN-S_8/CNT shows severe capacity fading (Figure S8b).

To probe the reaction mechanism of SPAN/CNT in the Li_2S_8-added ether electrolyte, the ex situ spectroscopic and morphological measurements of the electrode were performed upon the first discharge (1st-DC, 1.0 V) and recharge (1st-RC, 3.0 V) at 200 mA g^{-1} (Figure 3a). The cycled electrodes were washed by DME solvent thoroughly to remove the residual electrolyte and lithium salts for further characterizations. The peaks at ca. 27°, 32°, 45°, and 53° in the XRD patterns of the 1st-DC electrode indicate the formation of Li_2S product (Figure 3b). When recharging to 3.0 V, the characteristic peaks of Li_2S disappear, and instead, the peaks of S_8 are detected. Compared to the Raman spectrum of the pristine SPAN/CNT cathode, the signals assigned to C−S/S−S bonds become hardly detectable at 1st-DC and reappeared at 1st-RC (Figure 3c). The breakage and reconstruction of the C−S/S−S bonds suggest the reversibility of SPAN/CNT. To further clarify the chemical states of sulfur, high-resolution S 2p XPS was performed (Figure S9). For pristine SPAN/CNT, the peak at 164.6 eV is the response of the S−S bond.[35] The peaks located at 162.8 and 161.6 eV relate to the single C−S bond, and that at 163.4 eV corresponds to C−S of the short-chain organosulfide.[33] For the electrode of the 1st-DC, the S−S peak disappears, while there is a notable peak at 160 eV assigned to Li_2S, which is consistent with the result of XRD.[47] The C−S signals are still detectable, indicating the residual S in the backbone. In other words, it suggests that the S−S chains broke first before the C−S bonds, which should be due to the lower dissociation energy of S−S (251 kJ mol^{-1}) than that of the C−S bond (272 kJ mol^{-1}).[58] Upon the first recharge, the peak of S−S reappears and the relative intensities of the C−S peaks increase, indicating that the C−S/S−S bonds are able to be reconstructed during the delithiation process.

The SEM images of the 1st-DC electrode show that the nanofibers are covered thoroughly by Li_2S nanoflakes (Figure 3d), which disappear after the charge process (Figure 3e). In combination with the XRD, Raman, XPS and SEM characterizations, it is concluded that both SPAN and S_8 are formed at the end of the inverse charging. This means that the Li_2S undergoes two conversion pathways during the charge process by introducing Li_2S_8 in the electrolytes. The two competing reactions cooperate to promote the oxidation of Li_2S. The Li_2S_8 acting as a RM to chemically oxidize Li_2S and facilitate its electrochemical oxidation, leading to accelerated reaction kinetics. The mechanism is different from that in the work by Warneke et al., who proposed a promising hybrid system that benefitted from reversible sulfur incorporation into the SPAN structure with concomitant involvement of dimethyl trisulfide.[61] When using the base electrolytes, the lithiation products of SPAN are a mixture of Li_2S and Li coordinated polymer backbone (PAN-Li) upon the first discharge (Figure S10).[35] According to the aforementioned detectable C−S signals in the XPS result after the first discharge, partial C−S bonds are kept after the lithiation of SPAN. Wang et al. suggested that the full desulfurization of SPAN would not occur, as evidenced by a residual N/S ratio (mol/mol) of ca. 1:1 after the discharge at 167.5 mA g^{-1}.[62] With consideration that the desulfurization depth of SPAN would be affected by the applied current density, we prepared a series of SPAN/CNT cathodes that discharged in a range from 10 to 200 mA g^{-1} (Figure S11). The discharged electrodes were extensively washed in deionized water to remove the electrolyte and Li_2S products. The elemental analysis on the thoroughly dried

https://doi.org/10.1021/acsami.1c06004
ACS Appl. Mater. Interfaces 2021, 13, 25002−25009

electrodes suggests that residual S content in the backbone is dependent on the applied current density (Table S3). The S content is ca. 5.68 wt %, and the atomic ratio of N/S is ca. 2.36 after the first discharge at 10 mA g^{-1}, suggesting that the full desulfurization of SPAN is difficult even at a low current density. The produced Li_2S could not smoothly decompose during the delithiation process due to a high energy barrier. Yang et al. have shown that the Li_2S_8 additive would reduce the potential barrier of Li_2S significantly in the system with a Li_2S cathode.[57] The reaction pathway was the same as that for a S_8 cathode after the initial charge process. However, the electrochemical reaction process of a SPAN cathode is different. As illustrated in Figure 4, the presence of Li_2S_8 provides a new pathway to activate Li_2S. It could be assumed that the charging of Li_2S includes both electrochemical and chemical reactions. Soluble Li_2S_8 could oxidize the solid Li_2S by a chemical reaction to form Li_2S_n, which could be further electrochemically oxidized into both S_8 and C−S/S−S bonds of the partially lithiated SPAN upon recharge. Briefly, the two competing reactions cooperate to promote the conversion of Li_2S. In subsequent cycles, S_8 could reversibly convert to Li_2S_8 on discharge, which would continue to act as the chemical mediator on recharge. Therefore, Li_2S_8 can work continuously to guarantee decent battery performance.

4. CONCLUSIONS

In summary, a trace amount of Li_2S_8 was employed in ether-based electrolytes to regulate the reaction kinetics of the SPAN cathode material. The Li_2S products generated during dishcarge can be chemically oxidized by the Li_2S_8 additive, which facilitates the electrochemical oxidation of Li_2S upon recharge. The combined material and electrochemical characteristics have confirmed the transformation of both C−S/S−S bonds in SPAN and S_8 after the charge process, demonstrating the two conversion pathways of Li_2S. As a result, significantly boosted battery performance of SPAN/CNT is achieved with an enhanced initial CE of 82.9% at 200 mA g^{-1} and a steady capacity retention of 1170 mAh g^{-1} at 1000 mA g^{-1} after 400 cycles. Hence, the strategy of this study provides a competitive solution for building a highly efficient battery system with SPAN cathode materials.

■ ASSOCIATED CONTENT

Supporting Information

The Supporting Information is available free of charge at https://pubs.acs.org/doi/10.1021/acsami.1c06004.

Galvanostatic voltage profiles of SPAN synthesized at different temperatures; elemental analysis, TGA curves, CV curves, and EIS spectra of SPAN/CNT cathode in base or Li_2S_8-containing ether electrolyte; initial voltage profiles of SPAN/CNT at current densities of 200−2000 mA g^{-1}; comparison of the recently reported SPAN-based electrodes; cyclic performance of SPAN/CNT with a sulfur loading of 2 or 4 mg cm^{-2}; cyclic performance of pPAN/CNT with Li_2S_8-containing electrolyte; electrochemical characteristics of pPAN-S_8/CNT in base electrolyte; S 2p XPS spectra of SPAN/CNT at different discharge−charge states; voltage profiles and elemental analysis of SPAN/CNT after the first discharge at various current densities (PDF)

■ AUTHOR INFORMATION

Corresponding Author

Lina Wang − *State Key Laboratory for Modification of Chemical Fibers and Polymer Materials, College of Materials Science and Engineering, Donghua University, Shanghai 201620, P. R. China;* orcid.org/0000-0002-2211-4661; Email: linawang@dhu.edu.cn

Authors

Huilan Li − *State Key Laboratory for Modification of Chemical Fibers and Polymer Materials, College of Materials Science and Engineering, Donghua University, Shanghai 201620, P. R. China*

Wenying Xue − *State Key Laboratory for Modification of Chemical Fibers and Polymer Materials, College of Materials Science and Engineering, Donghua University, Shanghai 201620, P. R. China*

Tianxi Liu − *State Key Laboratory for Modification of Chemical Fibers and Polymer Materials, College of Materials Science and Engineering, Donghua University, Shanghai 201620, P. R. China; Key Laboratory of Synthetic and Biological Colloids, Ministry of Education, School of Chemical and Material Engineering, Jiangnan University, Wuxi 214122, P. R. China*

Complete contact information is available at: https://pubs.acs.org/10.1021/acsami.1c06004

Notes

The authors declare no competing financial interest.

■ ACKNOWLEDGMENTS

The authors acknowledge funding support from the National Natural Science Foundation of China (21603030) and the Shanghai Scientific and Technological Innovation Project (18JC1410600).

■ REFERENCES

(1) Manthiram, A.; Fu, Y.; Chung, S.-H.; Zu, C.; Su, Y.-S. Rechargeable Lithium-Sulfur Batteries. *Chem. Rev.* **2014**, *114*, 11751−11787.

(2) Yin, Y.-X.; Xin, S.; Guo, Y.-G.; Wan, L.-J. Lithium-Sulfur Batteries: Electrochemistry, Materials, and Prospects. *Angew. Chem., Int. Ed.* **2013**, *52*, 13186−13200.

(3) Yang, Y.; Zheng, G.; Cui, Y. Nanostructured Sulfur Cathodes. *Chem. Soc. Rev.* **2013**, *42*, 3018−3032.

(4) Chen, Y.; Gao, X.; Su, D.; Wang, C.; Wang, G. Accelerating Redox Kinetics of Lithium-Sulfur Batteries. *Trends in Chemistry* **2020**, *2*, 1020−1033.

(5) Chen, Y.; Zhang, W.; Zhou, D.; Tian, H.; Su, D.; Wang, C.; Stockdale, D.; Kang, F.; Li, B.; Wang, G. Co-Fe Mixed Metal Phosphide Nanocubes with Highly Interconnected-Pore Architecture as an Efficient Polysulfide Mediator for Lithium-Sulfur Batteries. *ACS Nano* **2019**, *13*, 4731−4741.

(6) Sun, M.; Wang, X.; Wang, J.; Yang, H.; Wang, L.; Liu, T. Assessment on the Self-Discharge Behavior of Lithium-Sulfur Batteries with $LiNO_3$-Possessing Electrolytes. *ACS Appl. Mater. Interfaces* **2018**, *10*, 35175−35183.

(7) Wang, L.; Zhao, Y.; Thomas, M. L.; Byon, H. R. In Situ Synthesis of Bipyramidal Sulfur with 3D Carbon Nanotube Framework for Lithium-Sulfur Batteries. *Adv. Funct. Mater.* **2014**, *24*, 2248−2252.

(8) Wang, J.; Fu, C.; Wang, X.; Yao, Y.; Sun, M.; Wang, L.; Liu, T. Three-dimensional Hierarchical Porous TiO_2/graphene Aerogels as Promising Anchoring Materials for Lithium-Sulfur Batteries. *Electrochim. Acta* **2018**, *292*, 568−574.

(9) Chung, S.-H.; Manthiram, A. Current Status and Future Prospects of Metal-Sulfur Batteries. *Adv. Mater.* **2019**, *31*, 1901125.
(10) Ji, X.; Nazar, L. F. Advances in Li-S Batteries. *J. Mater. Chem.* **2010**, *20*, 9821−9826.
(11) Zhao, C.; Yang, H.; Wang, X.; Li, H.; Qi, C.; Wang, L.; Liu, T. Effect of Soluble Sulfur Species on Electrochemical Behavior of Lithium-Sulfur Batteries with Dual-phase Electrolytes. *Sustainable Energy Fuels* **2019**, *3*, 1966−1970.
(12) Wang, L.; Liu, J.; Yuan, S.; Wang, Y.; Xia, Y. To Mitigate Self-discharge of Lithium-Sulfur Batteries by Optimizing Ionic Liquid Electrolytes. *Energy Environ. Sci.* **2016**, *9*, 224−231.
(13) Song, J.; Guo, X.; Zhang, J.; Chen, Y.; Zhang, C.; Luo, L.; Wang, F.; Wang, G. Rational Design of Free-standing 3D Porous MXene/RGO Hybrid Aerogels as Polysulfide Reservoirs for High-Energy Lithium-Sulfur Batteries. *J. Mater. Chem. A* **2019**, *7*, 6507−6513.
(14) Lee, J. S.; Kim, W.; Jang, J.; Manthiram, A. Sulfur-Embedded Activated Multichannel Carbon Nanofiber Composites for Long-Life, High-Rate Lithium-Sulfur Batteries. *Adv. Energy Mater.* **2017**, *7*, 1601943.
(15) Duan, B.; Wang, W.; Wang, A.; Yuan, K.; Yu, Z.; Zhao, H.; Qiu, J.; Yang, Y. Carbyne Polysulfide as a Novel Cathode Material for Lithium/Sulfur Batteries. *J. Mater. Chem. A* **2013**, *1*, 13261−13267.
(16) Xiao, D.; Li, Q.; Zhang, H.; Ma, Y.; Lu, C.; Chen, C.; Liu, Y.; Yuan, A. Sulfur Host Based on Cobalt-Graphitic Carbon Nanocages for High Performance Lithium-Sulfur Batteries. *J. Mater. Chem. A* **2017**, *5*, 24901−24908.
(17) Chen, K.; Sun, Z.; Fang, R.; Shi, Y.; Cheng, H.-M.; Li, F. Metal-Organic Frameworks (MOFs)-Derived Nitrogen-Doped Porous Carbon Anchored on Graphene with Multifunctional Effects for Lithium-Sulfur Batteries. *Adv. Funct. Mater.* **2018**, *28*, 1707592.
(18) Kim, S. H.; Yeon, J. S.; Kim, R.; Choi, K. M.; Park, H. S. A Functional Separator Coated with Sulfonated Metal-Organic Framework/Nafion Hybrids for Li-S Batteries. *J. Mater. Chem. A* **2018**, *6*, 24971−24978.
(19) Zhang, Y.; Zong, X.; Zhan, L.; Yu, X.; Gao, J.; Xun, C.; Li, P.; Wang, Y. Double-Shelled Hollow Carbon Sphere with Microporous Outer Shell towards High Performance Lithium-Sulfur Battery. *Electrochim. Acta* **2018**, *284*, 89−97.
(20) Chen, M.; Zhao, X.; Li, Y.; Zeng, P.; Liu, H.; Yu, H.; Wu, M.; Li, Z.; Shao, D.; Miao, C.; Chen, G.; Shu, H.; Pei, Y.; Wang, X. Kinetically Elevated Redox Conversion of Polysulfides of Lithium-Sulfur Battery using a Separator Modified with Transition Metals Coordinated g-C_3N_4 with Carbon-conjugated. *Chem. Eng. J.* **2020**, *385*, 123905.
(21) Wang, L.; Yang, Z.; Nie, H.; Gu, C.; Hua, W.; Xu, X.; Chen, X.; Chen, Y.; Huang, S. A Lightweight Multifunctional Interlayer of Sulfur-Nitrogen Dual-doped Graphene for Ultrafast, Long-life Lithium-Sulfur Batteries. *J. Mater. Chem. A* **2016**, *4*, 15343−15352.
(22) Qi, C.; Xu, L.; Wang, J.; Li, H.; Zhao, C.; Wang, L.; Liu, T. Titanium-Containing Metal-Organic Framework Modified Separator for Advanced Lithium-Sulfur Batteries. *ACS Sustainable Chem. Eng.* **2020**, *8*, 12968−12975.
(23) Li, H.; Wang, X.; Qi, C.; Zhao, C.; Fu, C.; Wang, L.; Liu, T. Self-assembly of MoO_3-Decorated Carbon Nanofiber Interlayers for High-Performance Lithium-Sulfur Batteries. *Phys. Chem. Chem. Phys.* **2020**, *22*, 2157−2163.
(24) Zhang, L.; Chen, X.; Wan, F.; Niu, Z.; Wang, Y.; Zhang, Q.; Chen, J. Enhanced Electrochemical Kinetics and Polysulfide Traps of Indium Nitride for Highly Stable Lithium-Sulfur Batteries. *ACS Nano* **2018**, *12*, 9578−9586.
(25) Yuan, Z.; Peng, H.-J.; Hou, T.-Z.; Huang, J.-Q.; Chen, C.-M.; Wang, D.-W.; Cheng, X.-B.; Wei, F.; Zhang, Q. Powering Lithium-Sulfur Battery Performance by Propelling Polysulfide Redox at Sulfiphilic Hosts. *Nano Lett.* **2016**, *16*, 519−527.
(26) Wang, J.; Yang, J.; Wan, C.; Du, K.; Xie, J.; Xu, N. Sulfur Composite Cathode Materials for Rechargeable Lithium Batteries. *Adv. Funct. Mater.* **2003**, *13*, 487−492.
(27) Zhang, S. S. Understanding of Sulfurized Polyacrylonitrile for Superior Performance Lithium/Sulfur Battery. *Energies* **2014**, *7*, 4588−4600.
(28) Chen, X.; Peng, L.; Wang, L.; Yang, J.; Hao, Z.; Xiang, J.; Yuan, K.; Huang, Y.; Shan, B.; Yuan, L.; Xie, J. Ether-compatible Sulfurized Polyacrylonitrile Cathode with Excellent Performance Enabled by Fast Kinetics via Selenium Doping. *Nat. Commun.* **2019**, *10*, 1021.
(29) Yu, X.; Xie, J.; Yang, J.; Huang, H.; Wang, K.; Wen, Z. Lithium Storage in Conductive Sulfur-Containing Polymers. *J. Electroanal. Chem.* **2004**, *573*, 121−128.
(30) Mukkabla, R.; Buchmeiser, M. R. Cathode Materials for Lithium-Sulfur Batteries Based on Sulfur Covalently Bound to a Polymeric Backbone. *J. Mater. Chem. A* **2020**, *8*, 5379−5394.
(31) Fanous, J.; Wegner, M.; Grimminger, J.; Andresen, Ä.; Buchmeiser, M. R. Structure-Related Electrochemistry of Sulfur-Poly(acrylonitrile) Composite Cathode Materials for Rechargeable Lithium Batteries. *Chem. Mater.* **2011**, *23*, 5024−5028.
(32) Warneke, S.; Eusterholz, M.; Zenn, R. K.; Hintennach, A.; Dinnebier, R. E.; Buchmeiser, M. R. Differences in Electrochemistry between Fibrous SPAN and Fibrous S/C Cathodes Relevant to Cycle Stability and Capacity. *J. Electrochem. Soc.* **2018**, *165*, A6017−A6020.
(33) Wei, S.; Ma, L.; Hendrickson, K. E.; Tu, Z.; Archer, L. A. Metal-Sulfur Battery Cathodes Based on PAN-Sulfur Composites. *J. Am. Chem. Soc.* **2015**, *137*, 12143−12152.
(34) Wang, L.; He, X.; Li, J.; Chen, M.; Gao, J.; Jiang, C. Charge/discharge Characteristics of Sulfurized Polyacrylonitrile Composite with Different Sulfur Content in Carbonate Based Electrolyte for Lithium Batteries. *Electrochim. Acta* **2012**, *72*, 114−119.
(35) Wang, X.; Qian, Y.; Wang, L.; Yang, H.; Li, H.; Zhao, Y.; Liu, T. Sulfurized Polyacrylonitrile Cathodes with High Compatibility in Both Ether and Carbonate Electrolytes for Ultrastable Lithium-Sulfur Batteries. *Adv. Funct. Mater.* **2019**, *29*, 1902929.
(36) Liu, Y.; Wang, W.; Wang, J.; Zhang, Y.; Zhu, Y.; Chen, Y.; Fu, L.; Wu, Y. Sulfur Nanocomposite as a Positive Electrode Material for Rechargeable Potassium-Sulfur Batteries. *Chem. Commun.* **2018**, *54*, 2288−2291.
(37) Zhang, Y.; Zhao, Y.; Yermukhambetova, A.; Bakenov, Z.; Chen, P. Ternary Sulfur/Polyacrylonitrile/$Mg_{0.6}Ni_{0.4}O$ Composite Cathodes for High Performance Lithium/Sulfur Batteries. *J. Mater. Chem. A* **2013**, *1*, 295−301.
(38) Páez Jerez, A. L.; Chemes, D. M.; Sham, E. L.; Davies, L. E.; Tesio, A. Y.; Flexer, V. Low-Temperature Synthesis of a Sulfur-Polyacrylonitrile Composite Cathode for Lithium-Sulfur Batteries. *Chemistry Select* **2020**, *5*, 5465−5472.
(39) Hwang, J.-Y.; Kim, H. M.; Sun, Y.-K. High Performance Potassium-Sulfur Batteries Based on a Sulfurized Polyacrylonitrile Cathode and Polyacrylic Acid Binder. *J. Mater. Chem. A* **2018**, *6*, 14587−14593.
(40) Liu, Y.; Haridas, A. K.; Lee, Y.; Cho, K.-K.; Ahn, J.-H. Freestanding Porous Sulfurized Polyacrylonitrile Fiber as a Cathode Material for Advanced Lithium Sulfur Batteries. *Appl. Surf. Sci.* **2019**, *472*, 135−142.
(41) Konarov, A.; Gosselink, D.; Doan, T. N. L.; Zhang, Y.; Zhao, Y.; Chen, P. Simple, Scalable, and Economical Preparation of Sulfur-PAN Composite Cathodes for Li/S Batteries. *J. Power Sources* **2014**, *259*, 183−187.
(42) Ye, J.; He, F.; Nie, J.; Cao, Y.; Yang, H.; Ai, X. Sulfur/carbon Nanocomposite-Filled Polyacrylonitrile Nanofibers as a Long Life and High Capacity Cathode for Lithium-Sulfur Batteries. *J. Mater. Chem. A* **2015**, *3*, 7406−7412.
(43) Huang, X.; Liu, J.; Huang, Z.; Ke, X.; Liu, L.; Wang, N.; Liu, J.; Guo, Z.; Yang, Y.; Shi, Z. Flexible Free-Standing Sulfurized Polyacrylonitrile Electrode for Stable Li/Na Storage. *Electrochim. Acta* **2020**, *333*, 135493.
(44) Kim, I.; Kim, C. H.; Choi, S. h.; Ahn, J.-P.; Ahn, J.-H.; Kim, K.-W.; Cairns, E. J.; Ahn, H.-J. A Singular Flexible Cathode for Room Temperature Sodium/Sulfur Battery. *J. Power Sources* **2016**, *307*, 31−37.

https://doi.org/10.1021/acsami.1c06004
ACS Appl. Mater. Interfaces 2021, 13, 25002−25009

(45) Frey, M.; Zenn, R. K.; Warneke, S.; Muller, K.; Hintennach, A.; Dinnebier, R. E.; Buchmeiser, M. R. Easily Accessible, Textile Fiber-Based Sulfurized Poly(acrylonitrile) as Li/S Cathode Material: Correlating Electrochemical Performance with Morphology and Structure. *ACS Energy Lett.* **2017**, *2*, 595−604.
(46) Yin, L.; Wang, J.; Yu, X.; Monroe, C. W.; NuLi, Y.; Yang, J. Dual-Mode Sulfur-Based Cathode Materials for Rechargeable Li-S Batteries. *Chem. Commun.* **2012**, *48*, 7868−7870.
(47) Jin, Z.-Q.; Liu, Y.-G.; Wang, W.-K.; Wang, A.-B.; Hu, B.-W.; Shen, M.; Gao, T.; Zhao, P.-C.; Yang, Y.-S. A New Insight into the Lithium Storage Mechanism of Sulfurized Polyacrylonitrile with no Soluble Intermediates. *Energy Storage Mater.* **2018**, *14*, 272−278.
(48) Yin, L.; Wang, J.; Lin, F.; Yang, J.; Nuli, Y. Polyacrylonitrile/Graphene Composite as a Precursor to a Sulfur-Based Cathode Material for High-Rate Rechargeable Li-S Batteries. *Energy Environ. Sci.* **2012**, *5*, 6966−6972.
(49) Wang, X.-G.; Zhang, Z.; Zhang, Q.; Wang, C.; Zhang, X.; Xie, Z.; Zhou, Z. $MoCl_5$ as a Dual-Function Redox Mediator for Li-O_2 Batteries. *J. Mater. Chem. A* **2019**, *7*, 14239−14243.
(50) Liu, T.; Kim, G.; Jonsson, E.; Castillo-Martinez, E.; Temprano, I.; Shao, Y.; Carretero-Gonzalez, J.; Kerber, R. N.; Grey, C. P. Understanding LiOH Formation in a Li-O_2 Battery with LiI and H_2O Additives. *ACS Catal.* **2019**, *9*, 66−77.
(51) Lim, H. D.; Song, H.; Kim, J.; Gwon, H.; Bae, Y.; Park, K.-Y.; Hong, J.; Kim, H.; Kim, T.; Kim, Y. H.; Lepró, X.; Ovalle-Robles, R. O.; Baughman, R. H.; Kang, K. Superior Rechargeability and Efficiency of Lithium-Oxygen Batteries: Hierarchical Air Electrode Architecture Combined with a Soluble Catalyst. *Angew. Chem.* **2014**, *126*, 4007−4012.
(52) Zhang, T.; Liao, K.; He, P.; Zhou, H. A Self-Defense Redox Mediator for Efficient Lithium-O_2 Batteries. *Energy Environ. Sci.* **2016**, *9*, 1024−1030.
(53) Zhang, W.; Shen, Y.; Sun, D.; Huang, Z.; Zhou, J.; Yan, H.; Huang, Y. Promoting Li_2O_2 Oxidation via Solvent-Assisted Redox Shuttle Process for Low Overpotential Li-O_2 Battery. *Nano Energy* **2016**, *30*, 43−51.
(54) Zhao, Q.; Katyal, N.; Seymour, I. D.; Henkelman, G.; Ma, T. Vanadium (III) Acetylacetonate as an Efficient Soluble Catalyst for Li-O_2 Battery. *Angew. Chem., Int. Ed.* **2019**, *58*, 12553−12557.
(55) Tsao, Y.; Lee, M.; Miller, E. C.; Gao, G.; Park, J.; Chen, S.; Katsumata, T.; Tran, H.; Wang, L.-W.; Toney, M. F.; Cui, Y.; Bao, Z. Designing a Quinone-Based Redox Mediator to Facilitate Li_2S Oxidation in Li-S Batteries. *Joule* **2019**, *3*, 872−884.
(56) Wu, X.; Liu, N.; Guan, B.; Qiu, Y.; Wang, M.; Cheng, J.; Tian, D.; Fan, L.; Zhang, N.; Sun, K. Redox Mediator: A New Strategy in Designing Cathode for Prompting Redox Process of Li-S Batteries. *Adv. Sci.* **2019**, *6*, 1900958.
(57) Yang, Y.; Zheng, G.; Misra, S.; Nelson, J.; Toney, M. F.; Cui, Y. High-Capacity Micrometer-Sized Li_2S Particles as Cathode Materialsfor Advanced Rechargeable Lithium-Ion Batteries. *J. Am. Chem. Soc.* **2012**, *134*, 15387−15394.
(58) Hwang, T. H.; Jung, D. S.; Kim, J.-S.; Kim, B. G.; Choi, J. W. One-Dimensional Carbon-Sulfur Composite Fibers for Na-S Rechargeable Batteries Operating at Room Temperature. *Nano Lett.* **2013**, *13*, 4532−4538.
(59) Wang, L.; Chen, X.; Li, S.; Yang, J.; Sun, Y.; Peng, L.; Shan, B.; Xie, J. Effect of Eutectic Accelerator in Selenium-doped Sulfurized Polyacrylonitrile for High Performance Room Temperature Sodium-Sulfur Batteries. *J. Mater. Chem. A* **2019**, *7*, 12732−12739.
(60) Lebherz, T.; Frey, M.; Hintennach, A.; Buchmeiser, M. R. Influence of Morphology of Monolithic Sulfur-Poly(acrylonitrile) Composites used as Cathode Materials in Lithium-Sulfur Batteries on Electrochemical Performance. *RSC Adv.* **2019**, *9*, 7181−7188.
(61) Warneke, S.; Zenn, R. K.; Lebherz, T.; Müller, K.; Hintennach, A.; Starke, U.; Dinnebier, R. E.; Buchmeiser, M. R. Hybrid Li/S Battery Based on Dimethyl Trisulfide and Sulfurized Poly-(acrylonitrile). *Adv. Sustainable Syst.* **2018**, *2*, 1700144.
(62) Wang, P.; Trück, J.; Niesen, S.; Kappler, J.; Küster, K.; Starke, U.; Ziegler, F.; Hintennach, A.; Buchmeiser, M. R. High-Performance Magnesium-Sulfur Batteries Based on a Sulfurated Poly(acrylonitrile) Cathode, a Borohydride Electrolyte, and a High-Surface Area Magnesium Anode. *Batteries and Supercaps* **2020**, *3*, 1239−1247.

https://doi.org/10.1021/acsami.1c06004
ACS Appl. Mater. Interfaces 2021, 13, 25002−25009